

## Accepted Manuscript

Precise geochronological constraints on the origin, setting and incorporation of ca. 1.59 Ga surficial facies into the Olympic Dam Breccia Complex, South Australia

Alexander R. Cherry, Kathy Ehrig, Vadim S. Kamenetsky, Jocelyn McPhie, James L. Crowley, Maya B. Kamenetsky

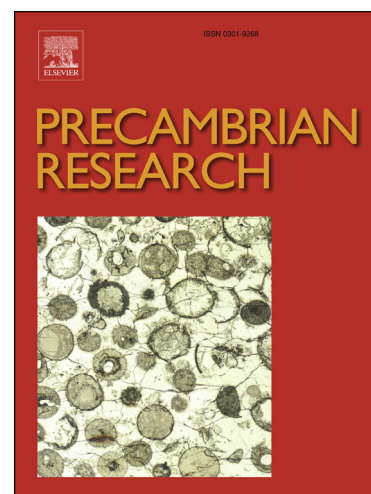
PII: S0301-9268(18)30111-6  
DOI: <https://doi.org/10.1016/j.precamres.2018.07.012>  
Reference: PRECAM 5132

To appear in: *Precambrian Research*

Received Date: 23 February 2018  
Revised Date: 8 July 2018  
Accepted Date: 17 July 2018

Please cite this article as: A.R. Cherry, K. Ehrig, V.S. Kamenetsky, J. McPhie, J.L. Crowley, M.B. Kamenetsky, Precise geochronological constraints on the origin, setting and incorporation of ca. 1.59 Ga surficial facies into the Olympic Dam Breccia Complex, South Australia, *Precambrian Research* (2018), doi: <https://doi.org/10.1016/j.precamres.2018.07.012>

This is a PDF file of an unedited manuscript that has been accepted for publication. As a service to our customers we are providing this early version of the manuscript. The manuscript will undergo copyediting, typesetting, and review of the resulting proof before it is published in its final form. Please note that during the production process errors may be discovered which could affect the content, and all legal disclaimers that apply to the journal pertain.



## Precise geochronological constraints on the origin, setting and incorporation of ca. 1.59 Ga surficial facies into the Olympic Dam Breccia Complex, South Australia

Alexander R. Cherry<sup>1,\*</sup>, Kathy Ehrig<sup>2</sup>, Vadim S. Kamenetsky<sup>1</sup>, Jocelyn McPhie<sup>1</sup>, James L. Crowley<sup>3</sup>, and Maya B. Kamenetsky<sup>1</sup>

<sup>1</sup>ARC Centre of Excellence in Ore Deposits (CODES), School of Natural Sciences, University of Tasmania, Hobart, Tasmania 7005, Australia

<sup>2</sup>BHP Olympic Dam, 55 Grenfell Street, Adelaide, South Australia 5000, Australia

<sup>3</sup>Department of Geosciences, Boise State University, 1910 University Drive, Boise, Idaho 83725, United States

### Abstract

The Olympic Dam Breccia Complex (host to the Olympic Dam Cu-U-Au-Ag deposit) is derived largely from granite (Roxby Downs Granite) but includes clasts and domains derived from surficial facies (felsic volcanic rocks and bedded clastic facies). New high-precision CA-TIMS geochronology is used to constrain the ages of the granite, the volcanic rocks and bedded clastic facies. The felsic volcanic rocks ( $1594.73 \text{ Ma} \pm 0.30 \text{ Ma}$ ) are slightly older than the granite ( $1593.87 \text{ Ma} \pm 0.21 \text{ Ma}$ ). These ages, together with the absence of any older country rock in the breccia complex, suggest the felsic volcanic rocks that were originally present at Olympic Dam were intruded by the granite. The deposition of the bedded clastic facies (tuffaceous mudstone) has been constrained to  $1590.97 \pm 0.58 \text{ Ma}$ , indicating the presence of a basin around 3 myr after emplacement of the granite and felsic volcanic rocks. Extrusive correlatives of mafic-ultramafic dykes intruding the breccia complex are proposed as a local source of detrital Cr-spinel in the bedded clastic facies. The granitoid-dominated provenance of some of the bedded clastic facies implies that ca. 1590 Ma granitoids were exposed when the bedded clastic facies were accumulating; the absence of  $\geq 1740 \text{ Ma}$  detrital zircons

indicates the provenance did not extend beyond granitoids of the Burgoyne Batholith in the vicinity of Olympic Dam. An initial stratigraphic sequence is proposed for the BCF involving a transition in provenance from volcanic-dominated to granitoid-dominated. Faults are proposed to have been responsible for the segmentation and incorporation of the bedded clastic facies into the Olympic Dam Breccia Complex. The formation of the Olympic Dam Breccia Complex and Olympic Dam hydrothermal system post-dated the emplacement of the Roxby Downs Granite (at  $1593.87 \pm 0.21$  Ma). The bedded clastic facies ( $1590.97 \pm 0.58$  Ma) have been altered and mineralised.

### **Keywords**

CA-TIMS, geochronology, Roxby Downs Granite, Gawler Range Volcanics, Olympic Dam, bedded clastic facies

## **1. Introduction**

The Olympic Dam (OD) Cu-U-Au-Ag deposit is one of the largest in the world; current total resources have been estimated at over 10.1 Gt (0.78% Cu, 0.25 kg/t  $U_3O_8$ , 0.33 g/t Au, 1 g/t Ag) (BHP, 2017). Based on limited drill-hole information, OD was first described as a type of “sediment-hosted ore deposit” (Roberts and Hudson, 1983; p. 799). Successive studies following additional drilling and underground development reinterpreted the deposit to be hosted within a breccia complex (Olympic Dam Breccia Complex - ODBC) inside a granite pluton (Roxby Downs Granite - RDG) and suggested a “hydrothermal-tectonic” origin for the breccia complex (Oreskes and Einaudi, 1990; Reeve et al., 1990). The ODBC mainly comprises clasts of variably hematite-altered granite; clasts of mafic-ultramafic, felsic volcanic (correlated with the

Gawler Range Volcanics - GRV) and various bedded clastic facies are locally the dominant clast-type (Reeve et al., 1990). Domains of bedded clastic facies have gradational or faulted contacts with the ODBC and are internally deformed (McPhie et al., 2011; Ehrig et al., 2012).

The bedded clastic facies (BCF) are well bedded and overall relatively fine-grained (McPhie et al., 2011). The origin of the BCF is a major aspect of two contrasting models of the architecture, early setting and relative timing of formation of the ODBC and deposit (Oreskes and Einaudi, 1990; Reeve et al., 1990; Johnson and Cross, 1995; McPhie et al., 2011; Ehrig et al., 2012; McPhie et al., 2016). Reeve et al. (1990) suggested the BCF occurred within “localised diatreme structures” and represented deposits from explosive venting of the OD hydrothermal system (p. 1017). This model proposed that the BCF were derived from the ODBC as “reworked hydrothermal eruption breccias” and locally from the GRV (Reeve et al., 1990; p. 1033). Johnson and Cross (1995) dated samples thought to be from the diatreme structures and felsic dykes that post-dated mineralisation with the intent of determining a minimum age of the OD orebody. The diatreme model has had a significant influence on work on the age, and fluid and metal sources of OD, as well as on strategies of exploration for similar deposits (e.g. Oreskes and Einaudi, 1992; Haynes et al., 1995; Johnson and Cross, 1995; Johnson and McCulloch, 1995; Skirrow et al., 2007; Hayward and Skirrow, 2010). The alternative model proposed the BCF were remnants of a sedimentary basin that overlay the ODBC (Oreskes and Einaudi, 1990; McPhie et al., 2011) and that the OD hydrothermal system may have interacted with the overlying basin (McPhie et al., 2011; McPhie et al., 2016).

This study reports precise zircon CA-TIMS geochronology to constrain the ages and relationships of the BCF, the RDG and volcanic rocks (GRV) in the ODBC. The new ages indicate the RDG probably intruded the GRV at OD and that the BCF were deposited around 3 myr after emplacement of the GRV and RDG. The earliest timing of formation of the ODBC and OD hydrothermal system is constrained by the age of the RDG. The BCF are brecciated and contain hydrothermal minerals, implying that tectonic and hydrothermal activity was occurring after ca. 1591 Ma. Additional insights into the provenance of the BCF are provided, based on Cr-spinel compositional data, LA-ICPMS geochronology, and descriptions and interpretations of previous workers. The above data and interpretations (including those of previous workers) are used to propose an original stratigraphy of the surficial facies (BCF and GRV) and a model of their incorporation into the ODBC.

## **2. Geological setting**

The Gawler Craton is dominated by late Archaean, Palaeoproterozoic and early Mesoproterozoic successions (Fig. 1a) (Drexel et al., 1993; Hand et al., 2007). The late Archaean Mulgathing and Sleaford Complexes (~2500 Ma) occupy the central-northern and southern portions of the craton, respectively (Hand et al., 2007). The Palaeoproterozoic Hutchison Group (~2000-1866 Ma) and Donington Suite (~1850 Ma) occur in the south and east, whereas the metasedimentary Wallaroo Group (~1760-1740 Ma) occurs along the eastern margin of the craton (Hand et al., 2007). These units were deformed in the Kimban orogeny (~1730-1690 Ma); the Archaean units were also affected by the earlier Sleafordian (~2480-2420 Ma) orogeny (Hand et al., 2007).

The granitoid Hiltaba Suite and co-magmatic GRV constitute an early Mesoproterozoic (~1590 Ma) silicic large igneous province (the Gawler SLIP; Allen et al., 2008; McPhie et al., 2008). The GRV are widespread over the central and eastern Gawler Craton and are subdivided into the upper GRV (thick, voluminous felsic lavas, ca. 1587 Ma) and lower GRV (very thick but spatially restricted felsic and subordinate mafic volcanic units, 1595-1587 Ma) (Blissett et al., 1993). The contemporaneous Benagerie Volcanic Suite in the Curnamona Province to the west of the Gawler Craton (Wade et al., 2012) indicates earliest Mesoproterozoic magmatism also extended beyond the Gawler Craton. Sedimentary successions of GRV age or related to GRV volcanism occur at Roopena (~270 km S of Olympic Dam; Curtis et al., 2018), Prominent Hill (~150 km NW of Olympic Dam; Bull et al., 2015) and OD (Reeve et al., 1990). The Hiltaba Suite comprises predominantly granitic batholiths and plutons, though there is considerable compositional variation including the presence of minor mafic plutons (Flint, 1993). Evidence of deformation associated with emplacement of the Hiltaba Suite is summarised by Hand et al. (2007), who suggested it was restricted to contractional shear zones striking northwest-southeast in the western part of the Gawler Craton.

The eastern Gawler Craton and Gawler SLIP are unconformably overlain by the Mesoproterozoic (ca. 1.4 Ga) red-bed Pandurra Formation (Fanning et al., 1983; Preiss, 1987; Cowley, 1991; Cherry et al., 2017). The Pandurra Formation is, in turn, unconformably overlain by the Neoproterozoic to Cambrian Stuart Shelf sedimentary formations (Preiss, 1993, 2000). Mafic dykes of the Gairdner Dolerite dyke swarm intruded the northern and eastern Gawler Craton during the Neoproterozoic (ca. 830 Ma; Wingate et al., 1998).

### 3. Geology of Olympic Dam

The OD deposit is entirely contained within the ODBC, which is enclosed by the RDG (Fig. 1b), a member of the Hiltaba Suite (Reeve et al., 1990; Johnson and Cross, 1995).

The main components in the ODBC are derived from the surrounding RDG and hydrothermal sources (Reeve et al., 1990). Brecciated felsic and mafic/ultramafic GRV (Reeve et al., 1990; Huang et al., 2016) and BCF (McPhie et al., 2011) are also present and are locally significant in the ODBC. Gairdner Dolerite dykes intrude the ODBC (Huang et al., 2015).

The ODBC-RDG boundary is gradational and marked by progressively altered and brecciated granite (Reeve et al., 1990). The margin of the ODBC is defined by Ehrig et al. (2012) as the altered envelope where igneous biotite is not preserved in the granite (1 to 5 km from the deposit centre). In detail, the ODBC comprises numerous, irregularly shaped breccia bodies that consist of differing proportions of hematite and altered granite protolith (Oreskes and Einaudi, 1990; Reeve et al., 1990). However, there is a systematic increase in intensity of brecciation and hydrothermal alteration (mainly in the form of hematite addition) from the margins inward (Reeve et al., 1990; Ehrig et al., 2012). The intensity of brecciation and alteration can be such that identification of many of the protolith lithologies in the ODBC (such as granite, BCF and felsic and mafic-ultramafic GRV correlatives) is difficult (Ehrig et al., 2012). The hematite (or Fe) content is used to subdivide the breccias within the ODBC (Reeve et al., 1990). Granite-rich breccia largely consists of angular granite clasts, a relatively minor hydrothermal component (e.g. hematite) and low proportion of matrix (Reeve et al., 1990). Hematite-rich breccia contains a much higher hydrothermal component relative to the granite component and matrix abundance increases with increasing hematite

content (Reeve et al., 1990; Ehrig et al., 2012). Some domains in the hematite-rich breccia contain abundant felsic volcanic clasts (felsic volcanic breccia), particularly in the vicinity of the large (up to 300 m across/thick) domains of BCF in the southern portion of the ODBC (McPhie et al., 2011; Ehrig et al., 2012). The felsic volcanic clasts in the felsic volcanic breccia are feldspar-phyrlic and have been suggested to be the incorporated remnants of felsic GRV units that were originally present above the RDG (Reeve et al., 1990; McPhie et al., 2011).

Sericite (muscovite, illite, phengite and minor paragonite) is widespread throughout the ODBC and is the dominant alteration phase in the outer portions of the ODBC (e.g. granite-rich breccia). Sericite has been replaced by hematite towards the centre of the deposit (Ehrig et al., 2012), where the breccias contain little other than hematite, quartz and barite (Fig. 1b) (Reeve et al., 1990). Magnetite is present around the margins and at depth in the deposit (Ehrig et al., 2012). Significant hydrothermal fluorite, barite, pyrite, quartz, siderite, apatite and chlorite also occur, amongst numerous other phases (Ehrig et al., 2012). The main ore minerals include Cu-Fe sulfides (chalcopyrite, bornite, and chalcocite-like group minerals (i.e. chalcocite, digenite, djurleite, roxbyite, anilite), U minerals (uraninite, coffinite and brannerite), electrum and many minor phases (Ehrig et al., 2012). The majority of the ore occurs in hematite-rich breccia, although significant ore may be associated with granite-rich breccia; the central hematite-quartz-barite breccia (Fig. 1b) is largely devoid of Cu and U minerals but locally contains important amounts of Au (Reeve et al., 1990; Ehrig et al., 2012). The deposit-wide zonation of Cu-Fe sulfides involves chalcopyrite-pyrite at depth and towards the margins of the deposit, and an overall transition to bornite-chalcocite at shallower levels and towards the centre of the deposit (Reeve et al., 1990).

The host granite, breccia complex and ore deposit are all unconformably overlain by 300 m of Stuart Shelf sedimentary formations, including the Tregolana Shale and a thin layer of Nuccaleena Dolomite immediately above the unconformity (Roberts and Hudson, 1983). The Pandurra Formation once overlies OD but is no longer preserved (Cherry et al., 2017).

#### **4. Bedded clastic facies (BCF)**

The general characteristics of the BCF are here summarised from previous authors; their main characteristics are most recently described by McPhie et al. (2016). The majority of the BCF within the ODBC are contained within two domains (Fig. 1b, c) that extend several hundred metres below the unconformity with Stuart Shelf formations; bedded clasts thought to be fragments of the BCF have been intersected in the ODBC over 1300 m below the unconformity (e.g. RD2786a, ~1900 m down hole). The southern domain is the largest and has an E-W extent of 1300 m and a vertical extent over 700 m (Fig. 1c) (McPhie et al., 2011). The northern domain is over 500 m long and its vertical extent is over 200 m. Both domains are over 300 m across (McPhie et al., 2016). Margins of the domains of BCF are faulted, obscured by hematite alteration or are gradational into the surrounding hematite breccia (McPhie et al., 2011). Some faults crosscutting the BCF are occupied by mafic dykes and intervals of hematite-rich breccia (McPhie et al., 2011).

Soft-sediment deformation of the BCF has resulted in locally disrupted beds and disharmonic folds and faults. Faults, contorted beds and broken drill-core commonly obscure the stratigraphic relationships within the BCF.

The facies associations discussed here are equivalent to those presented by McPhie et al. (2016): (1) green sandstone and mudstone, (2) interbedded sandstone and red mudstone,

(3) polymictic volcanic-clast conglomerate, (4) thinly bedded green and red mudstone, and (5) quartz-rich sandstone. A description of the detrital and secondary components of the BCF based on Ehrig et al. (2012), McPhie et al. (2011), (2016) and observed in this study is presented in Table S1 of the supplementary text and in Figures 2 to 5.

- (1) The green sandstone and mudstone facies association (Fig. 2) is a significant component of the southern domain of the BCF and consists of interlaminated sandstone and mudstone, and some thicker (1-10 m) sandstone beds, many of which contain intraformational mudstone clasts (McPhie et al., 2016).
- (2) The interbedded sandstone and red mudstone (Fig. 3) is a significant component of both the southern and northern domains of the BCF (McPhie et al., 2016). This facies association consists of red mudstone interbedded with pale sandstone and minor granule/pebble conglomerate or breccia beds (Ehrig et al., 2012; McPhie et al., 2016). The sandstone beds are internally massive, laminated, graded or cross-laminated; the cross laminae may be defined by heavy minerals.
- (3) The polymictic volcanic-clast conglomerate facies (Fig. 4) is present in both the northern and southern domains of the BCF (McPhie et al., 2016). The conglomerate beds are poorly sorted and internally massive, vary from clast- to matrix-supported, and are intersected as 3-70 m thick intervals in drill holes (Ehrig et al., 2012; McPhie et al., 2016). The majority of clasts in the conglomerate are rounded although some are angular and irregular (McPhie et al., 2016). The conglomerate matrix is referred to by Oreskes and Einaudi (1990), Reeve et al. (1990) and Johnson and Cross (1995) as pale, sericite-altered “volcanic lapilli and ash”. In contrast, McPhie et al. (2016) described the

conglomerate matrix as composed of polymictic volcanic sand-sized grains and also noted thin intervals of sandstone of similar composition intercalated with the conglomerate.

- (4) The thinly bedded green and red mudstone facies (Fig. 5) is a volumetrically minor component of the BCF (McPhie et al., 2016). This facies association consists mostly of laminated, red, hematite-rich mudstone that resembles banded iron formation (ironstone) (Fig. 5a-d) (Ehrig et al., 2012), and pale green tuffaceous mudstone that is internally massive or laminated and includes hematite-rich laminae (Fig. 5e-h) (Oreskes and Einaudi, 1990; Reeve et al., 1990; Johnson and Cross, 1995; McPhie et al., 2016). McPhie et al. (2016) reported the presence of altered bubble-wall glass shards in the tuffaceous mudstone. Laminated barite (Oreskes and Einaudi, 1990), interlaminated green and red mudstone, and beds of pale grey, brown and purple fine-grained sandstone are also included in this facies association (McPhie et al., 2016).
- (5) The quartz-rich sandstone facies was first reported by McPhie et al. (2016). Cherry et al. (2017) expanded description of the facies and correlated it with the ca. 1.4 Ga Pandurra Formation. This facies has been identified in only a few drill holes, near the southern domain of BCF. Contacts (where observed) between the quartz-rich sandstone and other BCF are always faulted. The intervals of this facies are strongly brecciated and comprise fragments of coarse-grained, quartz-rich sandstone suspended in a red-brown matrix of disaggregated sandstone. The sandstone fragments and red-brown matrix are dominated by quartz with granitoid and metamorphic characteristics, and also contain detrital muscovite,

tourmaline, zircon, hematite, ilmenite, and rutile. The sandstone fragments are cemented by quartz, illite and some hematite whereas the red-brown matrix contains abundant fine-grained hematite. The correlation of this facies with the Pandurra Formation indicates it is not related to the other BCF (Cherry et al., 2017) and so is not discussed further.

## 5. Zircon geochronology

The first zircon geochronology on the BCF at OD was conducted by Johnson and Cross (1995) on a sample of ‘diatreme tuff’ (probably equivalent to the tuffaceous mudstone component of the thinly bedded green and red mudstone) using the sensitive high-resolution ion microprobe (SHRIMP), which resulted in a  $^{207}\text{Pb}/^{206}\text{Pb}$  age of  $1597 \pm 8$  Ma ( $n = 26$ ). Jagodzinski (2005) analysed zircon in ‘volcaniclastic sandstone’ (correlated with the green sandstone and mudstone association), producing a SHRIMP  $^{207}\text{Pb}/^{206}\text{Pb}$  age of  $1594.5 \pm 3.3$  Ma ( $n = 20$ ). McPhie et al. (2016) reported laser ablation inductively coupled plasma mass spectrometry (LA-ICPMS) U-Pb ages of  $1590.6 \pm 3.2$  Ma ( $n = 139$ , combined interbedded sandstone and red mudstone and green sandstone and mudstone facies associations) and  $1603 \pm 10$  Ma ( $n = 24$ , felsic volcanic clasts in polymictic volcanic-clast conglomerate facies) from three samples of the BCF. Johnson and Cross (1995) also analysed clasts from two units of “autobrecciated felsic dykes” (interpreted here to be conglomeratic intervals in the BCF or domains of felsic volcanic breccia), yielding respective SHRIMP  $^{207}\text{Pb}/^{206}\text{Pb}$  ages of  $1592 \pm 8$  Ma ( $n = 19$ ) and  $1584 \pm 20$  Ma ( $n = 13$ ). Jagodzinski (2014) analysed zircon from the felsic volcanic breccia as well, producing a SHRIMP  $^{207}\text{Pb}/^{206}\text{Pb}$  age of  $1593 \pm 6$  Ma ( $n = 15$ ).

Jagodzinski (2014) also analysed the RDG (two sessions) and reported SHRIMP  $^{207}\text{Pb}/^{206}\text{Pb}$  ages of  $1594 \pm 5$  Ma ( $n = 27$ , session 1) and  $1594 \pm 7$  Ma ( $n = 20$ , session 2).

### 5.1. Method overview

Detailed descriptions of the geochronology methods used in this study are provided in the supplementary text. Samples were crushed, sieved and panned; zircons were handpicked from the resulting heavy mineral concentrate, mounted on 1-inch epoxy resin disks and polished. LA-ICPMS analysis was conducted at the University of Tasmania for single spot U-Pb zircon geochronology on samples of the BCF. The resulting ages were determined using Isoplot (Ludwig, 2008). The dataset of McPhie et al. (2016) was reprocessed with additional samples, including tuffaceous mudstone. Zircon grains were selected for chemical abrasion-thermal ionisation mass spectrometry (CA-TIMS) conducted at the Isotope Geology Laboratory at Boise State University, Idaho, from samples of RDG, tuffaceous mudstone, and felsic volcanic fragments from the polymictic volcanic-clast conglomerate, a conglomerate interval in the interbedded sandstone and red mudstone and from the domain of felsic volcanic breccia (e.g. Fig. 6) adjacent to the southern domain of the BCF. The samples are described in more detail in the supplementary text. Care was taken to avoid contamination from the matrix of BCF or breccia samples by crushing only the volcanic fragments. The RDG samples were selected from drill holes far from the ODBC to minimise the potential alteration of zircons by the OD hydrothermal system. The high precision dates from CA-TIMS analysis were used to interpret and distinguish igneous crystallisation ages of the RDG and the GRV source(s) of the analysed samples. A one-way analysis of variance (ANOVA) was conducted on the CA-TIMS sample data to determine if any

heterogeneity between the mean ages is statistically significant and was followed by Tukey-Kramer pairwise comparisons to determine which samples differed.

## 5.2. Results

### 5.2.1. LA-ICPMS geochronology

Detrital zircons in the BCF are euhedral to subhedral grains (up to 200  $\mu\text{m}$ ) and angular fragments; oscillatory zonation is common. Many grains are internally fractured, particularly in the tuffaceous mudstone (Fig. 5f). Single spot analyses were conducted on 460 zircon grains from the BCF. The number and drill holes of the analysed samples are presented in Table S4 of the supplementary text. Filtering for analyses that were highly discordant (metamict) and/or with elevated  $^{204}\text{Pb}$  (indicative of the presence of common Pb) resulted in 346 grains being considered suitable for age interpretation. Data are presented in Table D1 of the supplementary dataset. The vast majority of the zircons in each of the BCF associations have ca. 1.59 Ga ages, as was noted by the prior studies listed above. The intercept dates for the BCF associations are (reporting random and total, including systematic, uncertainties ( $2\sigma$ ); Horstwood et al., 2016):  $1592.3 \pm 6.9 \pm 17.6$  Ma for the interbedded sandstone and red mudstone ( $n = 143/219$ , MSWD = 1.3, probability of fit – p.o.f = 0.018, Fig. 7a),  $1590.3 \pm 7.4 \pm 17.8$  Ma for the green sandstone and mudstone ( $n = 89/108$ , MSWD = 0.77, p.o.f = 0.94, Fig. 7b),  $1588.2 \pm 11 \pm 19.5$  Ma for the tuffaceous mudstone ( $n = 62/79$ , MSWD = 2.5, p.o.f = 0.000, Fig. 7c), and  $1603.7 \pm 11 \pm 19.6$  Ma for felsic volcanic clasts in the polymictic volcanic-clast conglomerate facies ( $n = 41/47$ , MSWD = 1.6, p.o.f = 0.010, Fig. 7d). Most of the intercept dates have mean square weighted deviations (MSWD) close to 1, which implies that the majority of the analyses in each facies association are within error

(within the resolution of the LA-ICPMS technique). The higher MSWD of the tuffaceous mudstone is likely to be due to the zircons from that facies being fractured and altered. A small population of analyses ( $n = 11$ ) comprising zircons from all facies associations except the polymictic volcanic-clast conglomerate recorded apparent older ages; 9 of the 11 analyses define a ca. 1700 Ma age (Fig. 7e).

### 5.2.2. CA-TIMS geochronology

The zircons were analysed from the samples listed in Table 2 and data are presented in Table D2 of the supplementary dataset. The results are summarised by lithology (and by sample where variation occurs) and include description of zircon texture (Fig. 8) and U-Pb dates. Isoplot 3.7 (Ludwig, 2008) was used to calculate weighted mean  $^{207}\text{Pb}/^{206}\text{Pb}$  dates from 5-8 equivalent dates per samples (i.e. p.o.f >0.05). The igneous crystallization ages are based on the weighted mean  $^{207}\text{Pb}/^{206}\text{Pb}$  dates rather than  $^{206}\text{Pb}/^{238}\text{U}$  dates due to some  $^{206}\text{Pb}/^{238}\text{U}$  dates being slightly to moderately younger, presumably due to Pb loss. Results are presented in Figures 9 and 10. All analyses except for two are <1.9% discordant; 69 of the 73 analyses are <0.6% discordant. Errors on the weighted mean dates are given at  $2\sigma$  and are the internal errors based on analytical uncertainties only, including counting statistics, subtraction of tracer solution, and blank and initial common Pb subtraction. The reported dates utilize the U decay constants recommended by Steiger and Jager (1977), including a  $^{238}\text{U}/^{235}\text{U}$  of 137.88. If a more recently determined  $^{238}\text{U}/^{235}\text{U}$  of 137.818 were used (Hiess et al., 2012),  $^{207}\text{Pb}/^{206}\text{Pb}$  dates would be younger by ~0.84 Ma.

**Table 2. Note: the CA-TIMS results for sample 200036 6176 were first reported in (Jagodzinski et al., 2016).**

Sample ID	Drill hole	Depth (m)	Lithology
OD1207	SSH255	426.4	GRV clast in felsic volcanic breccia
OD55	Grab sample from underground drive MJ54WEST		Large GRV clast in polymictic volcanic-clast conglomerate
OD487	RD1624	602.5	Large GRV clast in interbedded sandstone and red mudstone
OD1201	RD2488	681.9	RDG
OD1202	RD2499	814.1	RDG
OD1214	RD2284	352.8	RDG
OD1215	RD2499	529.7	RDG
200036 6176	RD575	531	RDG
OD239	RD3449	427.2	Tuffaceous mudstone
OD41	RD3449	429.8	Tuffaceous mudstone

#### *Gawler Range Volcanics (GRV)*

Sample OD55 is a felsic volcanic cobble collected from an underground drive in the polymictic volcanic-clast conglomerate association in the northern domain of the BCF.

Sample OD487 is a cobble from conglomerate within an interval of interbedded sandstone and red mudstone in the southern domain of the BCF. Sample OD1207 consists of a coarse felsic clast from the domain of felsic volcanic breccia (inferred to be the incorporated remnants of felsic GRV originally present above the RDG) adjacent to the southern domain of the BCF; the felsic volcanic fragments are surrounded by hematite-rich matrix. A single cobble was crushed separately for CA-TIMS analysis, after first removing the outer surface and any attached matrix. Zircons from the three felsic volcanic samples have simple cores with rims that show oscillatory and/or sector zones (Fig. 8a-c). More complex oscillatory zonation appears to be more common in the zircons from the felsic volcanic breccia sample (OD1207). Inclusions and patchy

zonation are evident in some grains in all three samples. Analysis of 7 zircons from each of the felsic volcanic samples resulted in weighted mean ages that agree within analytical uncertainty (Figs. 9 and 10): OD55 =  $1594.87 \pm 0.80$  Ma ( $n = 6/7$ , MSWD = 1.5, p.o.f = 0.18); OD487 =  $1594.52 \pm 0.52$  Ma ( $n = 7$ , MSWD = 0.49, p.o.f = 0.81); OD1207 =  $1594.78 \pm 0.56$  Ma ( $n = 7$ , MSWD = 0.50, p.o.f = 0.81). The oldest 6 zircons were used to produce the weighted mean date of OD55; one analysis has a young date ( $1591.2 \pm 1.2$  Ma) which is attributed to ancient Pb loss. These weighted mean dates are interpreted to represent the igneous crystallisation ages of the source GRV. Combining the analyses of all three samples produces a weighted mean age of  $1594.73 \pm 0.30$  Ma ( $n = 20$ , MSWD = 0.76, p.o.f = 0.75). The low MSWD and high probability of fit indicate the three samples are statistically very similar and likely to be of the same age population.

#### *Roxby Downs Granite (RDG)*

Many zircons from the five samples of RDG are fragments and most exhibit oscillatory zones; some grains have patchy and sector zones (Fig. 8d-h). Inclusions exist in many of the zircon grains. Grains with a bright CL response are inferred to be lower in U and consequently less damaged by decay of U and its unstable daughters. Analysis of up to 8 grains from each of the RDG samples resulted in weighted mean  $^{207}\text{Pb}/^{206}\text{Pb}$  dates that agree within analytical uncertainty (Figs. 9 and 10): OD1201 =  $1593.90 \pm 0.44$  Ma ( $n = 8$ , MSWD = 1.09, p.o.f = 0.37); OD1202 =  $1594.09 \pm 0.56$  Ma ( $n = 7$ , MSWD = 0.84, p.o.f = 0.54); OD1214 =  $1593.52 \pm 0.63$  Ma ( $n = 5/7$ , MSWD = 2.09, p.o.f = 0.079); OD1215 =  $1593.83 \pm 0.46$  Ma ( $n = 8$ , MSWD = 0.59, p.o.f = 0.76); 200036 6176 =  $1593.90 \pm 0.58$  Ma ( $n = 8$ , MSWD = 1.5, p.o.f = 0.16). Two analyses from OD1214

were not used in the weighted mean date: one is significantly older ( $1636.04 \pm 1.22$  Ma) indicating an inherited component and the other is highly discordant due to ancient Pb loss. Combining the analyses of all five samples yields a weighted mean of  $1593.87 \pm 0.21$  Ma ( $n = 36$ , MSWD = 1.08, p.o.f = 0.35) and is interpreted to be the igneous crystallisation age of the RDG. The good agreement among all of the samples (shown by the MSWD and probability of fit of the combined weighted mean age) suggests the RDG was not emplaced incrementally over a long period of time, at least not beyond the resolution afforded by the CA-TIMS method.

*Tuffaceous mudstone in the thinly bedded green and red mudstone facies association*

Samples OD41 and OD239 are from tuffaceous mudstone from the northern domain of the BCF. Both samples retain the bubble-wall shard texture identified by McPhie et al. (2016), despite being altered largely to sericite. Zircons are commonly fractured or fragmented; many intact grains are elongate (relative to those from the RDG and felsic volcanic samples). CL images revealed two distinct populations (those with a strong CL response and those with a suppressed response, Fig. 8i, j) which are inversely correlated with U concentration. Oscillatory, sector and patchy zonation are variably apparent. Analysis of 6 grains from sample OD41 and 11 grains from sample OD239 yielded similar weighted mean dates (Figs. 9 and 10): OD41 =  $1590.70 \pm 0.88$  Ma ( $n = 6$ , MSWD = 1.12, p.o.f = 0.35); OD239 =  $1591.19 \pm 0.80$  Ma ( $n = 5/8$ , MSWD = 0.87, p.o.f = 0.48). Combining the analyses of the two samples yields a weighted mean of  $1590.97 \pm 0.58$  Ma ( $n = 11$ , MSWD = 0.97, p.o.f = 0.46). A number of analyses from OD239 were not used for age interpretation: three were of poor quality (chemically abraded fragments too small to have sufficient radiogenic Pb for precise dates) and were

not considered, two others are highly discordant and gave significantly younger dates ( $1582.02 \pm 1.79$  and  $1575.84 \pm 1.63$  Ma) that are attributed to ancient Pb loss, and one had an older date ( $1595.67 \pm 2.13$  Ma) that is interpreted to indicate the presence of an inherited component or detrital zircon from reworking of the tuff or contamination of the sample. The increased number of rejected analyses is consistent with the higher MSWD of the weighted mean of the LA-ICPMS analyses.

## 6. Chromian spinel composition

Analyses of Cr-spinel grains from three samples of the green sandstone and mudstone were first reported by McPhie et al. (2011), and showed a wide scatter in trace element abundance. The scatter was interpreted by those authors as well as McPhie et al. (2016) to reflect the green sandstone and mudstone having a broad provenance that received Cr-spinel generated in multiple tectonic settings. The data presented here expand upon that dataset, providing additional Cr-spinel analyses from seven samples of the green sandstone and mudstone as well as from five samples of tuffaceous mudstone.

Chromian spinel occurs as free detrital grains (e.g. Fig. 5g) in both facies and as inclusions in olivine-phyric clasts (e.g. Fig. 2b) in the green sandstone and mudstone.

Chromian spinel grains were extracted from samples and mounted on epoxy resin disks in the same manner as the zircon grains. Compositions of Cr-spinel grains were determined with a Cameca SX100 electron microprobe (see supplementary text for details of the method). Multiple Cr-spinel grains in the additional samples of green sandstone and mudstone and tuffaceous mudstone were analysed. The geochemical filter ( $\text{ZnO} < 0.3$  wt.% and  $\text{MnO} < 0.6$  wt.%) used by Huang et al. (2016) to select for least-altered grains excluded only 4 of the total 273 analysed grains.

The analysed Cr-spinel grains from the green sandstone and mudstone have highly variable  $\text{TiO}_2$  and  $\text{Al}_2\text{O}_3$  compositions, on par with those previously reported by McPhie et al. (2011) (Fig. 11). Analyses of Cr-spinel from the tuffaceous mudstone have a more restricted composition range than those from the green sandstone and mudstone (Table D3 of the supplementary dataset). High compositional variability is shown by multiple grains in single samples and between samples. The compositional ranges of most samples overlap, whereas some samples have relatively restricted ranges (Fig. 11).

## 8. Discussion

### 8.1 Provenance of the BCF

#### 8.1.1. Felsic GRV

The ca. 1590 Ma age of nearly all detrital zircon in the BCF corresponds to the age of the Gawler SLIP (Fanning et al., 1988; Creaser and Cooper, 1993; Jagodzinski et al., 2016), which suggests the GRV and/or Hiltaba Suite granitoids were the primary or most significant sources of all of the BCF. A GRV/Hiltaba Suite-dominated provenance for the BCF has been suggested by a number of prior workers (Oreskes and Einaudi, 1990; Reeve et al., 1990; McPhie et al., 2016).

The felsic volcanic clasts in the BCF are described as “texturally, mineralogically and compositionally identical to ... the GRV” by McPhie et al. (2011; p. 796), consistent with the LA-ICPMS and CA-TIMS geochronology of the BCF. The domains of breccia composed primarily of felsic, feldspar-phyric volcanic clasts (e.g. Fig. 6) within the ODBC have been suggested to be the incorporated remnants of felsic GRV that was

originally present above the RDG (Reeve et al., 1990; McPhie et al., 2011). Indeed, the nearest intact felsic GRV known occur at the Acropolis prospect, approximately 20 km SW of OD (Creaser and Cooper, 1993). The CA-TIMS age of the felsic volcanic clast from the breccia (OD1207) is indistinguishable from the CA-TIMS ages of the felsic volcanic cobbles in the BCF (OD55 and OD487), as shown by the low MSWD and high probability of fit when analyses from all of the samples are combined (Fig. 10). The presence of felsic volcanic clasts in the BCF that are the same age as the felsic volcanic clast from the breccia suggests the GRV that was once present above the RDG (and probably present regionally) predated deposition of the BCF.

Comparison of CA-TIMS ages of the felsic volcanic samples with recent high-precision geochronology of the GRV throughout the Gawler Craton (Jagodzinski et al., 2016) has revealed that the GRV at OD was part of the lower GRV (1595-1587 Ma) as opposed to the upper GRV (ca. 1587 Ma). A number of the lower GRV samples from the Gawler Ranges dated by (Jagodzinski et al., 2016) have CA-TIMS ages that correspond closely with the age of the tuffaceous mudstone (ca. 1591 Ma). A lower GRV source is also consistent with the presence of quartz in the tuffaceous mudstone, as the upper GRV is primarily feldspar-phyric (Allen et al., 2008).

#### 8.1.2. *Mafic GRV*

A GRV origin or timing for the mafic volcanic clasts in the green sandstone and mudstone and the polymictic volcanic-clast conglomerate facies has been proposed by prior authors (Johnson and Cross, 1995; McPhie et al., 2011; McPhie et al., 2016) but direct dating of the mafic volcanic clasts has not been possible to confirm their age. The mafic volcanic clasts with pseudomorphed olivine phenocrysts are texturally similar to

olivine-phyric mafic dykes in the ODBC described by Huang et al. (2016). These dykes have been dated, by LA-ICPMS U-Pb geochronology of magmatic apatite, at ca. 1590 Ma and have been correlated with mafic lower GRV elsewhere in the Gawler Craton (Huang et al., 2016). The extrusive equivalents of these and similar mafic dykes may have been the source of the corresponding mafic volcanic clasts in the green sandstone and mudstone and the polymictic volcanic-clast conglomerate facies.

The highly variable compositions of the Cr-spinel in the green sandstone and mudstone were interpreted by McPhie et al. (2011) and (2016) to reflect contribution from multiple volcanic sources because Cr-spinel compositions have been shown to be sensitive indicators of different tectonic settings. In particular, TiO<sub>2</sub> and Al<sub>2</sub>O<sub>3</sub> composition of Cr-spinel varies with parental melt composition (Kamenetsky et al., 2001). The absence of any recognised local sources of Cr-spinel at the time also supported this interpretation. Huang et al. (2016) has since recognised GRV-age mafic dykes intruding the ODBC that contain pseudomorphed olivine phenocrysts with Cr-spinel inclusions. The presence of these dykes in the ODBC suggests these and similar dykes may have fed mafic volcanism in the vicinity of OD.

Analyses by Huang et al. (2016) of Cr-spinel from mafic units in the ODBC encompass significant compositional variation. A number of distinct compositional populations are present (Fig. 11) (see Table D3 of the supplementary dataset) that may each correspond to distinct parental melts. This variation in parental melt implies the presence of multiple magma sources in the vicinity of OD or the changing of parental melt composition of a single source over a relatively short period of time (e.g. Cr-spinel in Mt Etna; Kamenetsky and Clocchiatti, 1996). The compositions of Cr-spinel from mafic

units that have thus far been identified within the ODBC have a broadly similar range to the detrital Cr-spinel in the BCF (Fig. 11). However, they do not account for all of the Cr-spinel variation in the BCF. This relationship suggests that if the Cr-spinel in the BCF was locally derived, the volcanic source(s) had a greater compositional variation than indicated by the known GRV-age mafic units in the ODBC. Alternatively, the Cr-spinel population in the BCF could be a mixture from local and remote sources.

The presence of quartz, zircon and bubble-wall shards in the tuffaceous mudstone suggests the source magma was felsic (McPhie et al., 2016). The minor Cr-spinel grains in the tuffaceous mudstone were probably added via mixing with locally-derived mafic components during waterlain deposition. The Cr-spinel in the tuffaceous mudstone has a more restricted compositional range relative to the green sandstone and mudstone.

### 8.1.3. *Hiltaba Suite*

A Hiltaba Suite contribution (e.g. granite clasts, quartz, feldspar, and zircon) to the BCF has been proposed by numerous prior authors (Reeve et al., 1990; Johnson and Cross, 1995; McPhie et al., 2011; McPhie et al., 2016), in particular for the interbedded sandstone and red mudstone, although granite-derived quartz and granitic fragments are also present in other facies associations (e.g. green sandstone and mudstone, Fig. 2d).

Much of the componentry of the interbedded sandstone and red mudstone (e.g. quartz, feldspar, Fe oxide, accessory zircon, tourmaline, fluorite, apatite and rutile) is present in the Hiltaba Suite granitoids in the vicinity of OD (including the RDG) (Creaser, 1996).

The granitic components were probably contributed from Hiltaba Suite granitoids within the Burgoyne Batholith surrounding OD due to the absence of

Palaeoproterozoic-age detrital zircons from basement rocks surrounding the Burgoyne Batholith (i.e.  $\geq 1740$  Ma).

The occurrence of detrital hematite grains in the interbedded sandstone and red mudstone with remnant magnetite cores/patches (e.g. Fig. 3d) suggests that an unknown proportion of the hematite may have originally been magnetite. Magnetite is present as a primary accessory phase in the Hiltaba Suite granitoids in the vicinity of OD (Creaser, 1996) and Fe oxide may have also been present in the form of magnetite-hematite veins in exposed Hiltaba Suite (such as in the RDG; Ehrig et al., 2012) or Gawler Range Volcanics in the vicinity of OD (cf. the nearby Acropolis prospect).

#### 8.1.4. *The ODBC?*

Previous workers have suggested the ODBC was a source of clasts in the BCF (Oreskes and Einaudi, 1990; Reeve et al., 1990). Hematite in the laminated, hematite-rich mudstone (ironstone) of the thinly bedded green and red mudstone facies association has characteristics consistent with formation through detrital deposition (e.g. Fig 5b-c), chemical precipitation (e.g. Fig 5d) or hydrothermal replacement of tuffaceous material (Oreskes and Einaudi, 1990). Erosion of exposed hematite-altered RDG or hematite-rich breccia (which has an RDG protolith) could produce many of the detrital components observed in the interbedded sandstone and red mudstone facies association. However, no components have been identified that uniquely indicate the ODBC was a source of detritus to the BCF. Further work is required to narrow the range of probable source(s) of detrital components (particularly Fe-oxide) in the interbedded sandstone and red mudstone facies association.

#### 8.1.5. Palaeoproterozoic sources?

A very small population of zircons from three of the BCF associations defines an older age of ca. 1700 Ma (Fig. 7e). This older age population may indicate that some zircons had inherited components or that a Palaeoproterozoic source contributed to the BCF. However, the ca. 1700 Ma age does not correlate with known zircon populations in the Wallaroo Group ( $\geq 1740$  Ma) and Donington Suite (ca. 1850 Ma) that surround the Hiltaba Suite granitoids in the vicinity of OD (e.g. at Snake Gully, 10 km ENE of OD; Creaser, 1989; Jagodzinski, 2005). An inherited component or the presence of common Pb is suggested to be the probable cause of this ca. 1700 Ma population.

#### 8.2. Age of the BCF

The preservation of bubble-wall shard texture in the tuffaceous mudstone suggests its deposition was contemporaneous with or shortly after eruption; this texture would not survive significant reworking (Fisher and Schmincke, 1984). Polymictic volcanic-clast conglomerate facies adjacent to the tuffaceous mudstone has a tuff-like matrix (identification limited by intense sericite and/or hematite alteration of the matrix), which suggests the conglomerate may have been deposited at the same time as the tuffaceous mudstone or while the tuffaceous mudstone was still unconsolidated. The CA-TIMS age of zircon in the tuffaceous mudstone ( $1590.97 \pm 0.58$  Ma) is therefore taken to represent the timing of deposition of this facies and the other closely associated facies of the BCF. This result indicates that not only was a basin present above the GRV and RDG at this time but that the BCF are significantly younger than the GRV that underlay the basin.

### 8.3. Sulfides in the BCF

The same single or paired sulfide assemblages are present in all of the BCF associations, regardless of the detrital mineralogy of the facies being distinct, and in the ODBC (Fig. 2f-g, 3g-h, 5c, h-i) (e.g. pyrite-chalcopyrite, chalcopyrite-bornite, bornite-chalcocite; Ehrig et al., 2012). An exception is covellite which has replaced chalcocite (paired with bornite) in some BCF samples. Sulfides and associated hydrothermal phases (e.g. barite, fluorite and hematite) have morphologies and textures indicative of replacement and cavity-fill (e.g. Fig. 2f, 5c, h). The continuance of the same sulfide assemblage across facies and the ODBC as well as non-detrital textures indicate that sulfide deposition post-dates the deposition of the BCF (i.e. after 1591 Ma). The occurrence of sulfides occupying fractures/offsets of beds (e.g. Fig. 5c, h) suggests sulfide deposition took place after brittle deformation (i.e. potentially after lithification of the BCF).

### 8.4. Ages and relationships of the RDG and GRV at Olympic Dam

The timing of emplacement of the GRV at OD relative to the intrusion of the RDG has been a source of speculation (Oreskes and Einaudi, 1990; Reeve et al., 1990; McPhie et al., 2011; McPhie et al., 2016). The CA-TIMS ages of the GRV and RDG samples overlap (Fig. 10), and thus ages from single samples cannot determine which is older.

Combining all of the analyses to produce single weighted mean ages for the GRV ( $1594.73 \pm 0.30$  Ma, MSWD = 0.76, p.o.f = 0.75, n = 20) and RDG ( $1593.87 \pm 0.21$  Ma, MSWD = 1.08, p.o.f = 0.35, n = 5) reduces the  $2\sigma$  uncertainties of each sufficiently and suggests the RDG is distinguishably younger than the GRV (Fig. 10). Combining the analyses in this manner assumes that the RDG and the GRV supplying the clasts are both single entities (pluton and emplacement unit, respectively), a reasonable

presumption given that the sample ages for each unit are statistically indistinguishable (though the very small uncertainties of the combined ages are of uncertain statistical significance). The ANOVA also indicated the mean ages of the GRV and RDG samples are significantly heterogeneous, and the Tukey-Kramer pairwise comparison identified significant difference between the oldest GRV and youngest RDG samples (see Table D4 of the supplementary dataset).

Whether there was a contact (e.g. intrusive or unconformable) between the GRV and the RDG, or whether they were separated by older country rock is unknown. An unconformable contact implies the RDG would be significantly older than the GRV (to permit unroofing of the RDG prior to deposition of the GRV), which is precluded by the (potentially) older age of the GRV. Pre-1590 Ma (i.e. Palaeoproterozoic or earlier) zircons in the ODBC (as evidence of incorporation of older country rock) have not yet been recorded, aside from within fragments of the younger Pandurra Formation (Cherry et al., 2017) and potentially in the BCF (Fig. 7e, section 8.1.5). The absence of evidence (thus far) of pre-1590 Ma components in the ODBC is consistent with the RDG intruding already-present GRV. An intrusive contact was first suggested by Reeve et al. (1990) and intrusive contacts between Hiltaba Suite granites and the GRV occur elsewhere in the Gawler Craton (e.g. Flint, 1993; Agangi, 2011). Intrusion of the RDG into the GRV would require the RDG to have been shallowly emplaced (the thickest known preserved sections of lower GRV are up to 3 km thick, e.g. Chitanilga Volcanic Complex; Allen et al., 2008). Various textures indicative of shallow emplacement (e.g. miarolitic cavities, aplitic dikes, granophyric zones; Candela, 1997) were reported in the RDG by Creaser (1989). Kontonikas-Charos et al. (2017) suggested crystallisation pressures of ~2.2 kbar for the RDG, which corresponds to a depth of 6-8 km. However,

the barometer and thermometer used (i.e. Blundy and Holland, 1990; Anderson and Smith, 1995) have significant associated uncertainties (the barometer is highly temperature sensitive and the calculated temperatures have a  $2\sigma$  uncertainty of 75 °C, which imparts an uncertainty of up to 1.6 kbar to the calculated pressure) and the textural evidence for shallow emplacement is considered more reliable.

### **8.5. Setting and stratigraphy of the BCF**

The elongate, east-west, steeply dipping geometry of the southern BCF domain and of the separate facies associations (see Fig. 2 of McPhie et al., 2016) has been influenced by northeast- and northwest-striking fault sets (Hayward and Skirrow, 2010; McPhie et al., 2016). The original basin was proposed by McPhie et al. (2016) to have been defined by those same fault sets, partially on the basis of bedding measurements consistent with soft-sediment slumping down a palaeoslope with a northeasterly strike (dipping to the northwest or southeast).

Hematite-rich breccia, including domains of felsic volcanic breccia and hematite-quartz-barite breccia (characterised by intense, texturally destructive alteration of the protolith) occurs to the north of the main mass of the southern BCF domain (Fig. 1b) (Ehrig et al., 2012; McPhie et al., 2016). Juxtaposed to the south of the southern BCF domain is more granite-rich breccia, which then grades into unaltered RDG over a very short distance compared to elsewhere around the ODBC (Fig. 1b). Hayward and Skirrow (2010) noted the southern boundary of hematite-rich breccia, along which the southern BCF domain occurs, to be relatively planar and suggested it was influenced by a large, early northeast-striking fault zone. Significant vertical movement (i.e. north side up relative to the south) along this fault zone could account for the narrow transition to unaltered

RDG. The northern BCF domain was influenced by the same fault sets and has similar soft-sediment deformed bedding orientations as the southern BCF domain (McPhie et al., 2016), which suggests that it was originally part of the same basin. The northern BCF domain is also surrounded by a domain of hematite-quartz-barite breccia (Ehrig et al., 2012).

The southern BCF domain comprises multiple intervals of the different facies associations (Fig. 1c) (McPhie et al., 2016). Green sandstone and mudstone occurs in a thin northernmost interval that is adjacent to a segmented interval of interbedded sandstone and red mudstone (Fig. 1b, c). Portions of this interval (of interbedded sandstone and red mudstone) form an outlier separated by felsic volcanic breccia (Fig. 1b). Juxtaposed to the south of the interbedded sandstone and red mudstone is a second interval of green sandstone and mudstone; this interval is interbedded with polymictic volcanic-clast conglomerate and sandwiched to the south by a second interval of interbedded sandstone and red mudstone (Fig. 1c). The two intervals of the interbedded sandstone and red mudstone have been speculated by McPhie et al. (2016) to be either two distinct units or the result of fault repetition of a single unit. The presence of the northernmost interval of green sandstone and mudstone (also see Fig. 2C of McPhie et al., 2016) suggests that fault repetition is more likely, particularly considering the influence of faults on the geometry and segmentation of the BCF domains.

The presence of the felsic volcanic breccia domain immediately adjacent to the southern BCF domain (Fig. 1b) implies these surficial units were incorporated together. The significantly younger depositional timing of the BCF indicates the GRV (now felsic volcanic breccia) underlay the bedded clastic facies and suggests the north-to-south

sequence of felsic volcanic breccia, to green sandstone and mudstone and then interbedded sandstone and red mudstone may reflect the original stratigraphic sequence. Such a stratigraphy is consistent with initial emplacement of the GRV, followed by deposition of clastic facies with a GRV-dominated provenance and changing to clastic facies with a granitoid-dominated provenance (as Hiltaba Suite granite was exposed). Further work (e.g. a comprehensive study of younging directions) is required to unequivocally resolve the stratigraphy of the BCF.

#### **8.6. Incorporation of BCF and GRV into the ODBC**

The incorporation of the BCF has been discussed in only limited detail by prior workers; most attributed incorporation simply to downfaulting of the BCF as blocks into the ODBC (Oreskes and Einaudi, 1990; Hayward and Skirrow, 2010). McPhie et al. (2011) speculated that hydrothermal-tectonic brecciation was focussed on faults, and began in the RDG and propagated upward into the overlying GRV and BCF. The steeply dipping orientation of the southern domain of BCF and relationship to significant faults are features that, until now, have not been considered. The interpreted deposition and incorporation of the BCF and the GRV (felsic volcanic breccia) (Fig. 12) is constrained by the new geochronological and facies data and is summarised below.

1. The GRV and the RDG were emplaced at  $1594.73 \pm 0.30$  Ma and  $1593.87 \pm 0.21$  Ma, respectively. As indicated above (section 8.4.), the nature of the contact (if present) of the GRV and RDG is uncertain, although an intrusive contact is suggested to be the most likely scenario. The ODBC started to form after emplacement of the RDG and GRV, brecciation being focussed along early faults, and possibly propagating up towards the GRV.

2. Northeast- and northwest-striking faults are inferred to have been responsible for causing local subsidence above the RDG and GRV, defining a basin in which the BCF began to accumulate (e.g. McPhie et al., 2016). The presence of brecciated mafic-ultramafic GRV dykes in the ODBC indicates igneous activity continued after emplacement of the RDG; the dykes may have fed mafic volcanism in the vicinity of OD.

A distal(?) felsic eruptive centre produced a volcanic ash cloud that deposited tuffaceous mudstone in the basin at  $1590.97 \pm 0.58$  Ma. The low preservation potential of glass shards (and tuffaceous mudstone as a whole) in active sedimentary environments suggests the tuffaceous mudstone would have been best preserved in the central portions of the basin (away from the margins). The initial sediment input is suggested to have been dominated by felsic and mafic GRV sources and comprised a series of low- (green sandstone and mudstone) and high-energy (polymictic volcanic-clast conglomerate facies) depositional events. The sediments were likely deposited as fans or lobes near the margins of the basin, although some of the high-energy depositional events were of sufficient scale to deposit conglomerate with the tuffaceous mudstone farther out in the basin.

3. The erosion of the GRV exposed Hiltaba Suite (and possibly the RDG) in the BCF source area and led to a shift to a granitoid-dominated provenance (interbedded sandstone and red mudstone). The ca. 3 myr between the emplacement of the GRV and RDG, and the deposition of the BCF is likely to have been sufficient time to unroof Hiltaba Suite/RDG in the vicinity of OD. Detrital Fe oxide in the interbedded sandstone and red mudstone may have been derived from primary igneous Fe oxide and/or

magnetite-hematite veins. It is unknown whether exposed portions of the ODBC were available to contribute to the BCF due to uncertainty of the timing of the initiation of the ODBC.

4. The faults that originally defined the basin are here inferred to also be responsible for initiating incorporation of the BCF and underlying GRV into the ODBC. Orientation measurements on soft-sediment folds are consistent with slumping down a northeast-striking palaeoslope (McPhie et al., 2016); more pronounced vertical movement along the large, northeast-striking fault zone that defines the current southern margin of the BCF and hematite-rich breccia would be consistent with generating such a palaeoslope.

The progressive incorporation of the GRV and the BCF involved propagation of faults which led to brecciation and gradual segmentation into domains. The domains of the BCF were rotated by fault movement during incorporation, which steepened the dip of bedding in the BCF, particularly in the southern domain. The segmentation of the BCF led to the repetition of stratigraphy in the southern domain.

5. The RDG, ODBC and contained surficial lithologies (BCF and felsic volcanic breccia) were eroded and truncated by an unconformity overlain by the ca. 1440 Ma Pandurra Formation (Cherry et al., 2017). The Pandurra Formation was subsequently eroded and a second unconformity surface formed. This surface was overlain by post-glacial (Cryogenian?) sedimentary units of the Stuart Shelf, initially represented by facies indicative of a marine transgression (Nuccaleena Dolomite cap carbonate and Tregolana Shale; Williams, 1979; Reeve et al., 1990).

The timing of incorporation of the surficial units (BCF and felsic GRV) relative to hydrothermal alteration and mineralisation of the ODBC is not clear, save that the

surficial units are variably altered, mineralised and brecciated, which indicates there was tectonic and hydrothermal activity after ca. 1591 Ma. Any tectonic and hydrothermal activity that may have occurred prior to the BCF is currently constrained only by the emplacement of the RDG (at  $1593.87 \pm 0.20$  Ma).

## 9. Conclusions

Precise CA-TIMS zircon geochronology has shown that the GRV at OD ( $1594.73 \pm 0.30$  Ma) is slightly older than the RDG ( $1593.87 \pm 0.21$  Ma). The ODBC apparently lacks components older than either the RDG or the GRV, and textures in the RDG suggest that it was shallowly emplaced (Creaser, 1989). It is therefore most likely that at OD, the RDG intruded the GRV. The new age data support previous interpretations (McPhie et al., 2011) that the GRV at OD was originally overlain by the BCF; the GRV pre-dated deposition of the BCF ( $1590.97 \pm 0.58$  Ma) by about 3 myr. Hence, a basin was present at OD at least 3 myr after the RDG and GRV were emplaced. The initiation of brecciation and the hydrothermal system at OD post-dated the emplacement of the RDG. Because the BCF domains are partly brecciated and contain hydrothermal minerals (including sulfides), tectonic and hydrothermal activity took place after ca. 1591 Ma.

Cr-spinel in the BCF had previously been thought to indicate a regional provenance for lack of known local sources. Potential local sources of Cr-spinel with similar compositions are now known (e.g. extrusive correlates of mafic-ultramafic dykes intruding the ODBC). The Hiltaba Suite contribution to the BCF indicates that granite was unroofed somewhere in the source area by ca. 1591 Ma. Also, the absence of detrital Palaeoproterozoic zircons implies that the source was likely to have been from

granitoids within the Burgoyne Batholith (i.e. within a 40 x 80 km<sup>2</sup> area around OD). The detrital Fe oxide in the BCF was also probably derived from within the Burgoyne Batholith; possible sources include primary igneous Fe oxide and magnetite-hematite veins in granite. Because the timing of initiation of the ODBC has not been determined, it is not known whether exposed portions of the ODBC could have contributed Fe oxide to the BCF. An original stratigraphy is proposed as part of a model for the incorporation of the BCF into the ODBC, where a transition from a volcanic-dominated provenance to a granitoid-dominated provenance is inferred. Faults subsequently segmented and entrained the BCF into the ODBC.

### **Acknowledgements**

This paper represents part of the PhD project undertaken by A.R. Cherry while supported by an Australia Postgraduate Award scholarship. This project was funded by the Australian Research Council and BHP Olympic Dam. Discussions with M. Ferguson, N. Chapman, E. Jagodzinski, O. Apukhtina and Q. Huang are gratefully acknowledged. LA-ICPMS geochronology analysis and interpretation were assisted by S. Meffre and J. Thompson. Preparation of zircon for CA-TIMS was assisted by A. Edwards. Comments by E. Jagodzinski and an anonymous reviewer improved the quality of this manuscript.

### **References**

- Agangi, A., 2011, Magmatic and volcanic evolution of a silicic large igneous province (SLIP): the Gawler Range Volcanics and Hiltaba Suite, South Australia: University of Tasmania.
- Allen, S. R., McPhie, J., Ferris, G., and Simpson, C., 2008, Evolution and architecture of a large felsic igneous province in western Laurentia: The 1.6 Ga Gawler Range Volcanics, South Australia: *Journal of Volcanology and Geothermal Research*, v. 172, p. 132-147.

- Anderson, J. L., and Smith, D. R., 1995, The effects of temperature and fO<sub>2</sub> on the Al-in-hornblende barometer: *American Mineralogist*, v. 80, p. 549-559.
- BHP, 2017, Annual Report 2017, <<https://www.bhp.com/-/media/documents/investors/annual-reports/2017/bhpannualreport2017.pdf>>.
- Blissett, A. H., Creaser, R. A., Daly, S. J., Flint, R. B., and Parker, A. J., 1993, Gawler Range Volcanics, in Drexel, J. F., Preiss, W. V., and Parker A.J., eds., *The Geology of South Australia. Vol. 1, The Precambrian, Volume Bulletin 54: Geological Survey of South Australia*, p. 107-131.
- Blundy, J. D., and Holland, T. J. B., 1990, Calcic amphibole equilibria and a new amphibole-plagioclase geothermometer: *Contributions to Mineralogy and Petrology*, v. 104, p. 208-224.
- Bull, S., Meffre, S., Allen, M., Freeman, H., Tomkinson, M., and Williams, P., Volcanosedimentary and chronostratigraphic architecture of the host rock succession at Prominent Hill, South Australia, in *Proceedings SEG 2015: World-Class Ore Deposits: Discovery to Recovery, Hobart, Tasmania, Australia, September 27-30, 2015*, Society of Economic Geologists, p. 1.
- Candela, P. A., 1997, A review of shallow, ore-related granites: textures, volatiles and ore metals: *Journal of Petrology*, v. 38, p. 1619-1633.
- Cherry, A. R., McPhie, J., Kamenetsky, V. S., Ehrig, K., Keeling, J. L., Kamenetsky, M. B., Meffre, S., and Apukhtina, O. B., 2017, Linking Olympic Dam and the Cariewerloo Basin: Was a sedimentary basin involved in formation of the world's largest uranium deposit?: *Precambrian Research*, v. 300, p. 168-180.
- Cowley, W. M., 1991, The Pandurra Formation, Department of Mines and Energy, South Australia, open file Report Book 91/7, p. 45.
- Creaser, R. A., 1989, The geology and petrology of Middle Proterozoic felsic magmatism of the Stuart Shelf, South Australia [Ph.D thesis: La Trobe University].
- Creaser, R. A., 1996, Petrogenesis of a Mesoproterozoic quartz latite-granitoid suite from the Roxby Downs area, South Australia: *Precambrian Research*, v. 79, no. 3-4, p. 371-394.
- Creaser, R. A., and Cooper, J. A., 1993, U-Pb Geochronology of Middle Proterozoic Felsic Magmatism Surrounding the Olympic Dam Cu-U-Au-Ag and Moonta Cu-Au-Ag Deposits, South Australia: *Economic Geology*, v. 88, p. 186-197.
- Curtis, S., Wade, C., and Reid, A., 2018, Sedimentary basin formation associated with a silicic large igneous province: stratigraphy and provenance of the Mesoproterozoic Roopena Basin, Gawler Range Volcanics: *Australian Journal of Earth Sciences*, v. 65, p. 447-463.
- Drexel, J. F., Preiss, W. V., and Parker, A. J., 1993, The Geology of South Australia, Volume 1, The Precambrian: *Geological Survey of South Australia Bulletin*, v. 54, p. 242p.
- Ehrig, K., McPhie, J., and Kamenetsky, V. S., 2012, Geology and mineralogical zonation of the Olympic Dam Iron Oxide Cu-U-Au-Ag Deposit, South Australia, in Hedenquist, J. W., Harris, M., and Camus, F., eds., *Economic Geology Special Publication 16*, p. 237-267.
- Fanning, C. M., Flint, R. B., Parker, A. J., Ludwig, K. R., and Blissett, A. H., 1988, Refined Proterozoic evolution of the Gawler Craton, South Australia, through U-Pb zircon geochronology: *Precambrian Research*, v. 40, no. 41, p. 363-386.
- Fanning, C. M., Flint, R. B., and Preiss, W. V., 1983, Geochronology of the Pandurra Formation: *Geological Survey of South Australia Quarterly Geological Notes*, v. 88, p. 11-16.
- Fisher, R. V., and Schmincke, H.-U., 1984, *Pyroclastic Rocks*, Berlin, Springer-Verlag.
- Flint, R. B., 1993, Hiltaba Suite, in Drexel, J. F., Preiss, W. V., and A.J., P., eds., *The Geology of South Australia, Volume 1 The Precambrian, Volume 54: South Australia, Geological Survey Bulletin*.
- Hand, M., Reid, A., and Jagodzinski, L., 2007, Tectonic framework and evolution of the Gawler Craton, southern Australia: *Economic Geology*, v. 102, p. 1377-1395.

- Haynes, D. W., Cross, K. C., Bills, R. T., and Reed, M. H., 1995, Olympic Dam ore genesis: a fluid-mixing model: *Economic Geology*, v. 90, p. 281-307.
- Hayward, N., and Skirrow, R., 2010, Geodynamic setting and controls on iron oxide Cu-Au ( $\pm$ U) ore in the Gawler Craton, South Australia: Hydrothermal iron oxide copper-gold and related deposits: A global perspective, v. 3, p. 105-131.
- Hiess, J., Condon, D. J., McLean, N., and Noble, S. R., 2012,  $^{238}\text{U}/^{235}\text{U}$  systematics in terrestrial uranium-bearing minerals: *Science*, v. 335, p. 1610-1614.
- Horstwood, M. S. A., Košler, J., Gehrels, G., Jackson, S. E., McLean, N. M., Paton, C., Pearson, N. J., Sircombe, K., Sylvester, P., Vermeesch, P., Bowring, J. F., Condon, D. J., and Schoene, B., 2016, Community-derived standards for LA-ICP-MS U-(Th)-Pb geochronology - uncertainty propagation, age interpretation and data reporting: *Geostandards and Geoanalytical Research*, v. 20, p. 311-332.
- Huang, Q., Kamenetsky, V. S., Ehrig, K., McPhie, J., Kamenetsky, M., Cross, K., Meffre, S., Agangi, A., Chambefort, I., Direen, N. G., Maas, R., and Apukhtina, O., 2016, Olivine-phyric basalt in the Mesoproterozoic Gawler silicic large igneous province, South Australia: Examples at the Olympic Dam Cu-U-Au-Ag deposit and other localities: *Precambrian Research*, v. 281, p. 185-199.
- Huang, Q., Kamenetsky, V. S., McPhie, J., Ehrig, K., Meffre, S., Maas, R., Thompson, J., Kamenetsky, M., Chambefort, I., Apukhtina, O., and Hu, Y., 2015, Neoproterozoic (ca. 820-830 Ma) mafic dykes at Olympic Dam, South Australia: Links with the Gairdner Large Igneous Province: *Precambrian Research*, v. 271, p. 160-172.
- Jagodzinski, E. A., 2005, Compilation of SHRIMP U-Pb geochronological data - Olympic Domain, Gawler Craton, South Australia, 2001-2003, *in* Australia, G., ed., Volume Record 2005/20, p. 197 pp.
- Jagodzinski, E. A., 2014, The age of magmatic and hydrothermal zircon at Olympic Dam, Australian Earth Sciences Convention, Volume 110: Newcastle, Australia, Geological Society of Australia Abstracts, p. 260.
- Jagodzinski, E. A., Reid, A., Crowley, J., McAvaney, S. O., and Wade, C., 2016, Precise zircon U-Pb dating of a Mesoproterozoic silicic large igneous province: the Gawler Range Volcanics and Benagèric Volcanic Suite, South Australia, Australian Earth Sciences Convention, Volume 118: Adelaide, Australia, Geological Society of Australia, p. 494.
- Johnson, J. P., and Cross, K. C., 1995, U-Pb geochronological constraints on the genesis of the Olympic Dam Cu-U-Au-Ag deposit, South Australia: *Economic Geology*, v. 90, p. 1046-1063.
- Johnson, J. P., and McCulloch, M. T., 1995, Sources of mineralising fluids for the Olympic Dam deposit (South Australia) - Sm-Nd isotopic constraints: *Chemical Geology*, v. 121, no. 1-4, p. 177-199.
- Kamenetsky, V., and Clocchiatti, R., 1996, Primitive magmatism of Mt Etna: insights from mineralogy and melt inclusions: *Earth and Planetary Science Letters*, v. 142, p. 553-572.
- Kamenetsky, V. S., Crawford, A. J., and Meffre, S., 2001, Factors Controlling Chemistry of Magmatic Spinel: an Empirical Study of Associated Olivine, Cr-spinel and Melt Inclusions from Primitive Rocks: *Journal of Petrology*, v. 42, no. 4, p. 655-671.
- Kontonikas-Charos, A., Ciobanu, C. L., Cook, N. J., Ehrig, K., Krneta, S., and Kamenetsky, V. S., 2017, Feldspar evolution in the Roxby Downs Granite, host to Fe-oxide Cu-Au-(U) mineralisation at Olympic Dam, South Australia: *Ore Geology Reviews*, v. 80, p. 838-859.
- Ludwig, K. R., 2008, User's manual for Isoplot 3.70: A geochronological toolkit for Microsoft Excel: Berkeley Geochronological Center Special Publication, v. 4.
- McPhie, J., DellaPasqua, F., Allen, S. R., and Lackie, M. A., 2008, Extreme effusive eruptions: Palaeoflow data on an extensive felsic lava in the Mesoproterozoic Gawler Range

- Volcanics: *Journal of Volcanology and Geothermal Research*, v. 172, no. 1–2, p. 148-161.
- McPhie, J., Kamenetsky, V. S., Chambefort, I., Ehrig, K., and Green, N., 2011, Origin of the supergiant Olympic Dam Cu-U-Au-Ag deposit, South Australia: Was a sedimentary basin involved?: *Geology*, v. 39, p. 795-798.
- McPhie, J., Orth, K., Kamenetsky, V., Kamenetsky, M., and Ehrig, K., 2016, Characteristics, origin and significance of Mesoproterozoic bedded clastic facies at the Olympic Dam Cu-U-Au-Ag deposit, South Australia: *Precambrian Research*, v. 276, p. 85-100.
- Oreskes, N., and Einaudi, M. T., 1990, Origin of rare-earth element-enriched hematite breccias at the Olympic-Dam Cu-U-Au-Ag Deposit, Roxby Downs, South Australia: *Economic Geology*, v. 85, p. 1-28.
- Oreskes, N., and Einaudi, M. T., 1992, Origin of Hydrothermal Fluids at Olympic Dam: Preliminary Results from Fluid Inclusions and Stable Isotopes: *Economic Geology*, v. 87, p. 64-90.
- Preiss, W. V., 1987, Basement to the Adelaide Geosyncline, *in* Preiss, W. V., ed., *The Adelaide Geosyncline, late Proterozoic stratigraphy, sedimentation, palaeontology and tectonics, Volume 53: South Australia, Geological Survey of South Australia Bulletin*, p. 35-41.
- Preiss, W. V., 1993, Neoproterozoic, *in* Drexel, J. F., Preiss, W. V., and A.J., P., eds., *The geology of South Australia, Volume 1, the Precambrian, Volume 54: South Australia, Geological Survey of South Australia Bulletin*, p. 170-203.
- Preiss, W. V., 2000, The Adelaide Geosyncline of South Australia and its significance in Neoproterozoic continental reconstruction: *Precambrian Research*, v. 100, p. 21-63.
- Reeve, J. S., Cross, K. C., Smith, R. N., and Oreskes, N., 1990, Olympic Dam copper-uranium-gold-silver deposit, *in* Hughes, F. E., ed., *Geology of the mineral deposits of Australia and Papua New Guinea, Australasian Institute of Mining and Metallurgy, Melbourne, Monograph 14*, p. 1009-1035.
- Roberts, D. E., and Hudson, G. R. T., 1983, The Olympic Dam copper-uranium-gold deposit, Roxby Downs, South Australia: *Economic Geology*, v. 78, p. 799-822.
- Skirrow, R. G., Bastrakov, E. N., Baroncii, K., Fraser, G. L., Creaser, R. A., Fanning, C. M., Raymond, O. L., and Davidson, G. J., 2007, Timing of iron oxide Cu-Au-(U) hydrothermal activity and Nd isotope constraints on metal sources in the Gawler craton, South Australia: *Economic Geology*, v. 102, p. 1441-1470.
- Steiger, R. H., and Jager, E., 1977, Subcommission on geochronology: Convention on the use of decay constants in geo- and cosmochronology: *Earth and Planetary Science Letters*, v. 36, p. 359-362.
- Wade, C. E., Reid, A. J., Wingate, M. T. D., Jagodzinski, E. A., and Barovich, K., 2012, Geochemistry and geochronology of the c. 1585 Ma Benagerie Volcanic Suite, southern Australia: Relationship to the Gawler Range Volcanics and implications for the petrogenesis of a Mesoproterozoic silicic large igneous province: *Precambrian Research*, v. 206-207, p. 17-35.
- Williams, G. E., 1979, Sedimentology, stable-isotope geochemistry and palaeoenvironment of dolostones capping late Precambrian glacial sequences in Australia: *Journal of the Geological Society of Australia*, v. 26, p. 377-386.
- Wingate, M. T. D., Campbell, I. H., Compston, W., and Gibson, G. M., 1998, Ion microprobe U–Pb ages for Neoproterozoic basaltic magmatism in south-central Australia and implications for the breakup of Rodinia: *Precambrian Research*, v. 87, p. 135-159.

## Figure captions

- a.** Simplified pre-Neoproterozoic crystalline basement geology of the Gawler craton (after Hand et al., 2007). **b.** Plan view of the Olympic Dam deposit immediately below the unconformity showing simplified geology, including BCF and main ODBC domains. Deposit location is 30°26'25.225"S, 136°53'21.702"W; grid coordinates on the figure are referenced to GDA94/MGA zone 53 (after Ehrig et al., 2012). **c.** North-south cross-section of the western part of the southern BCF domain from McPhie et al. (2016) showing the multiple intervals of the different facies associations. RD2766, RD2767, RD2768, RD896, RU38-2625, RU38-2626 were the drill holes used by McPhie et al. (2016) to generate the cross-section.
- Green sandstone and mudstone. The following images highlight the clast types and hydrothermal assemblages; further detail of this facies association is presented in Table S1 of the supplementary text. **a.** Interbeds of sandstone and mudstone (RD896, 607.15 m). **b.** Olivine-phyric lithic clast with fine Cr-spinel inclusions (fine opaque grains in chlorite-altered olivine, arrow) (Plane polarised light - PPL, RD1627, 522.3 m). **c.** Angular reddish, hematite-altered felsic volcanic clast surrounded by various chlorite-altered mafic clasts (PPL, RU38-2625, 434.5 m). **d.** Granite clast with contained zircon grain (arrow) (PPL, RD1627, 522.3 m). **e.** Volcanic-derived quartz grain with large melt inclusion (arrow) (PPL, RU38-2626, 399 m). **f.** Chalcopyrite and pyrite replacement of an elongate clast (Reflected light - RL, RD1624, 538.8 m). **g.** Large euhedral pyrite crystals, commonly with porous/spongy cores. Minor associated chalcopyrite

(RL, RD1627, 738.4 m). **h.** Green sandstone and mudstone that has been hematite-altered (RD1628, ~430 m).

3. Interbedded sandstone and red mudstone. The following images highlight the clast types and hydrothermal assemblages; further detail of this facies association is presented in Table S1 of the supplementary text. **a.** Interbedded sandstone and mudstone; the grey bed to the upper right contains significant specular hematite. Cross-beds in the lower left of the image suggest at least some of the Fe oxide in this facies association is detrital (RD1989, 601.5 m). **b.** Fine-grained sandstone with abundant granitoid quartz grains (white), sericite-altered clasts (yellow-brown) and some opaque hematite grains. The bottom edge of the image shows the beginning of a band (bed?) dominated by opaque hematite grains (PPL, RD1625, 685.4 m). **c.** Two examples of large hematite grains; one elongate grain and a hematite-quartz aggregate (RL, RU38-2626, 338.3 m). **d.** Hematite grain with patches of remnant magnetite (arrow); a variety of hematite morphologies is apparent, including subrounded grains (RL, RD1625, 636.8 m). **e.** Heavy mineral band of hematite, zircon (arrows, Zr) and rutile (arrows, Ru) illustrating the probable detrital origin of at least some of the hematite in the bedded clastic facies (RL, RD1625, 685.4 m). **f.** Quartz sandstone with opaque, hematite-rich beds and cross-beds (arrows) (PPL, RU38-2625, 345.7 m). **g.** Sandstone bed with hematite-rich layer adjacent to mudstone. Bornite and chalcocite (orange and blue, respectively) are present throughout this sample interstitial to detrital grains but are most abundant in the sandstone bed (RL, RD1625, 679 m). **h.** False colour back scattered electron image of the

same sample as (g) showing the concentration of sulfide (yellow) in the sandstone beds relative to the mudstone beds (RL, RD1625, 679 m).

4. Polymictic volcanic-clast conglomerate. The following images highlight the clast types and hydrothermal assemblages; further detail of this facies association is presented in Table S1 of the supplementary text. **a.** Conglomerate with pale, tuff-like matrix. The dark, reddish clasts are feldspar-phyric and are derived from felsic volcanic rocks. A hematite-rich interval at the bottom of the image grades into tuffaceous mudstone (RD3449, 403-406 m). **b.** Conglomerate with a polymictic assemblage of both cobble and sand size clasts. Pale orange or dark reddish clasts are derived from felsic volcanic rocks and dark brown to green clasts have a mafic provenance (RU31-6018, 103.8 m). **c.** Hematite-altered conglomerate with very hematite-rich matrix. The dark red/brown or pale yellow colour of the clasts is attributed to hematite and sericite alteration, respectively (RD3449, 405.5 m). **d.** Hematite-altered clast with preserved lath-like texture presumed to represent an initial feldspar-phyric igneous texture (RL, RD2821, 668 m).
5. Thinly bedded green and red mudstone (tuffaceous mudstone and ironstone components of this facies association). Further detail of this facies association is presented in Table S1 of the supplementary text. **a.** Finely laminated ironstone comprising alternating red and grey hematite-rich beds. Sub-cm scale brittle offsets are apparent in the upper right of the image (RD3449, 462.1 m). **b.** A relatively coarse-grained ironstone bed containing abundant hematite adjacent to a very fine-grained mudstone bed (RL, RD3449, 409.3 m). **c.** Bornite (orange-yellow), chalcocite (blue) and barite (transparent, grey) in a brittle fracture of a

- hematite-rich ironstone bed (RL, RD3449, 462.5 m). **d.** Hematite grains (arrow, Hm) with remnant magnetite cores (Mt) in an ironstone bed; note the euhedral grain shapes consistent with the hematite being hydrothermal or diagenetic (RL, RD3449, 486.4 m). **e.** Pale green tuffaceous mudstone with fine-grained, hematite-rich laminae. Numerous brittle offsets are apparent in the sample (RD3449, 431.4 m). **f.** Euhedral, fractured zircon grain in tuffaceous mudstone (PPL, RD3449, 427.2 m). **g.** Angular quartz (Qz) and Cr-spinel (dark brown grain) in tuffaceous mudstone (PPL, RD3449, 427.2 m). **h.** Chalcocite (opaque, arrow, Cc) and fluorite (transparent/purple, arrow, Fl) occupying a brittle fracture in a hematite-rich lamina in tuffaceous mudstone (PPL, RD3449, 431.4 m). **i.** Disseminated chalcopyrite (yellow) and bornite (purple) and patches of very fine-grained hematite (reddish discoloration, arrow, Hm) in massive tuffaceous mudstone (RL, RD3449, 429.8 m).
6. Felsic volcanic breccia **a.** Sample with reddish, angular felsic volcanic fragments; thin pale rims on some of the fragments may be due to sericite alteration. Some specular hematite grains (grey) are present (RD2899, 409.7 m). **b.** Abundant grey hematite clasts. Felsic volcanic clasts are variably sericite- (pale, yellowish margins) or hematite-altered (reddish clasts) (RD647, 488.4 m).
7. Detrital zircon LA-ICPMS geochronology. **a.-d.** Tera-Wasserburg plots and intercept ages of the BCF, and **e.** Tera-Wasserburg plot of apparently older grains. Error ellipses are  $1\sigma$ ; reported uncertainties (internal and total, including systematic uncertainties) are  $2s$ .
8. Cathodoluminescence (CL) images of zircons used for CA-TIMS analysis, collected by a scanning electron microscope at Boise State University. Grain

- labels (e.g. z1, z2) correspond to the analysis number in the CA-TIMS dataset in the supplement (Table D2). Brightness of CL images is comparable within, but not between samples. **a.** OD1207 (SSH255, 426.4 m) – felsic volcanic breccia. **b.** OD55 (underground drive MJ54WEST grab sample) – polymictic volcanic clast-rich conglomerate. **c.** OD487 (RD1624, 602.5 m) – conglomerate interval in interbedded sandstone and red mudstone. **d.** OD1201 (RD2488, 681.9 m) – RDG. **e.** OD1202 (RD2499, 814.1 m) – RDG. **f.** OD1214 (RD2284, 352.8 m) – RDG. **g.** OD1215 (RD2499, 529.7 m) – RDG. **h.** 200036 6176 (RD575, 531 m) – RDG. **i.** OD239 (RD3449, 427.2 m) – tuffaceous mudstone. **j.** OD41 (RD3449, 429.8 m) – tuffaceous mudstone.
9. Wetherill concordia plots of CA-TIMS analyses for the zircons in Figure 8. Plots constructed using Isoplot 3.7 (Ludwig, 2008). The grey bands behind the concordia lines represent the decay constant uncertainty (to  $2\sigma$ ) of the concordia lines. Error ellipses are also  $2\sigma$ . Red ellipses in plots for OD55 and OD239 are excluded from age interpretation. Weighted mean ages of each sample are shown in Figure 10. Dashed lines separate each sample.
10. Ranked box plot of  $^{207}\text{Pb}/^{206}\text{Pb}$  dates (Ma) of the zircon CA-TIMS analyses. Black bars are single analyses, white bars are excluded analyses. Grey boxes behind bars are the weighted mean ages of each sample. Light grey boxes in front of the bars are combined weighted mean ages. Error bar and box height are  $2\sigma$ . Weighted mean ages determined using Isoplot 3.7 (Ludwig, 2008).
11. Bivariate  $\text{TiO}_2$  and  $\text{Al}_2\text{O}_3$  plot of Cr-spinel grains ( $n = 223$ ) in the BCF. The fields represent compositions of Cr-spinel from the altered mafic units in the ODBC presented by Huang et al. (2016): 1. Olivine-phyric lava/sill. 2. Olivine-

phyric basaltic dykes. 3. Olivine-phyric mafic unit samples originally collected by K. Cross.

12. Proposed model of incorporation of the BCF and felsic volcanic breccia into the ODBC; refer to Section 8.6 for explanation of each panel. The approximate location of the cross-section is shown on the plan view of the ODBC. Only faults inferred to be relevant to incorporation of the BCF and GRV into the ODBC are shown. The extent of Fe oxide development (after Ehrig et al., 2012) is shown only on panel 5 as the timing and distribution of Fe oxide in the ODBC is unknown relative to the deposition and incorporation of the BCF, save that the surficial units are variably altered and mineralised. The inferred intrusive relationship of the RDG and the GRV is shown on the right hand side of the panels in the form of the boundary between the GRV and the country rock being lower than the top of the RDG. The combined weighted mean ages of the GRV and RDG samples are also shown on panel 1. The 'Stuart Shelf' in the legend refers to the Neoproterozoic to Cambrian sedimentary formations of the Stuart Shelf that unconformably overlie the ODBC.

**Highlights**

- Age of host granite and surficial facies at Olympic Dam (OD) precisely constrained.
- The Roxby Downs Granite (~1594 Ma) intruded the Gawler Range Volcanics (~1595 Ma).
- Bedded clastic facies deposited at ~1591 Ma, ~3 myr after emplacement of granite.
- OD hydrothermal system post-dates ~1594 Ma granite and was active after 1591 Ma.
- Fault-controlled incorporation of surficial facies into breccia complex is proposed.